ChemPubSoc Europe

DOI: 10.1002/cphc.201800249

CHEMPHYSCHEM Communications

VIP *Very Important Paper*

Dramatic Decrease in CEST Measurement Times Using Multi-Site Excitation**

Tairan Yuwen,[a] Lewis E. Kay,[a, b] and Guillaume Bouvignies*[c]

Chemical exchange saturation transfer (CEST) has recently evolved into a powerful approach for studying sparsely populated, "invisible" protein states in slow exchange with a major, visible conformer. Central to the technique is the use of a weak, highly selective radio-frequency field that is applied at different frequency offsets in successive experiments, "searching" for minor state resonances. The recording of CEST profiles with enough points to ensure coverage of the entire spectrum at sufficient resolution can be time-consuming, especially for applications that require high static magnetic fields or when small chemical shift differences between exchanging states must be quantified. Here, we show – with applications involving ^{15}N CEST – that the process can be significantly accelerated by using a multi-frequency irradiation scheme, leading in some applications to an order of magnitude savings in measurement time.

Chemical exchange saturation transfer (CEST)[1,2] has emerged as a powerful NMR approach for studies of sparsely populated, transiently formed (excited) states of both proteins and nucleic acids.[3,4] A wide variety of CEST-based experiments have recently been developed for biomolecular applications that amplify signals from ^{15}N, ^{13}C or ^{1}H spin probes of excited states,[5] bringing into view conformers that are recalcitrant to study using other biophysical approaches. In the CEST experiment a weak B_1 field, typically between 10–50 Hz, is applied, one frequency at a time, so as to cover the frequency range of the resonances of interest (for example, between 105–135 ppm for amide ^{15}N spins) and the intensities of peaks from the major conformational (ground) state are quantified.[3] Consider, for simplicity a two-site exchange process involving the interconversion between ground and excited states, the latter often invisible in standard NMR spectra, with focus on a single spin A. When the B_1 field is applied on-resonance with the A ground state position its longitudinal magnetization is rapidly lost, often due to a saturation effect. Conversely, when the weak field is placed at the frequency of A in the excited state the resulting perturbation to longitudinal magnetization is transferred via chemical exchange to the ground state, so that the intensity of the ground state A correlation is reduced. Thus, a plot of the normalized intensity, I/I_o, as a function of the position of the B_1 field, where I and I_o are the ground state peak A intensities in the presence and absence of the B_1 irradiation period, respectively, produces a CEST profile with a pair of dips at the resonance positions of A in the major and minor states. Fits of the resulting profiles to the Bloch-McConnell equations describing chemical exchange[6] facilitate the extraction of the populations of the exchanging states, their rates of interconversion and, importantly, the chemical shifts of the spins in the excited state.

The inherent simplicity of the CEST experiment, whereby each frequency in the region of interest is interrogated one spectrum at a time by varying the position of a weak B_1 field and the effects on the ground state spectrum monitored, is also a weakness of the method. The number of spectra that must be recorded scales inversely with the strength of the applied B_1 field (ν_1 in Hz), with the spacing of B_1 fields between successive datasets on the order of ν_1.[5] In the case of ^{15}N-CEST applications this translates into approximately 60 spectra for a typical B_1 field of 25 Hz and a spectrometer operating at 500 MHz, and since each is of the 2D variety measurement times can be extensive. The situation becomes critical for studies of systems where chemical shift differences between spins in ground and excited states are small since then small B_1 fields must be employed (see below) and concomitantly larger numbers of spectra recorded. Notably, although CEST applications benefit from high magnetic fields that lead to increases in sensitivity and resolution in 2D read-out spectra, as well as to larger separations between major and minor dips in the CEST dimension, the increased frequency bandwidth that must therefore be covered results in large numbers of measured datasets and hence longer measurement times as well. Here we introduce a new CEST excitation scheme that effectively removes these limitations by exciting multiple spectral positions in the CEST domain simultaneously so that the number of points that must be recorded is significantly reduced. The utility of the methodology is demonstrated with applications to G48A Fyn SH3 and A39G FF domains that interconvert between folded and unfolded conformers.[7,8]

To record CEST datasets in an accelerated manner we make use of the DANTE selective excitation scheme, as first proposed by Bodenhausen, Freeman and Morris,[9] and illustrated in Figure 1a. Here, k rectangular pulses are applied at intervals of τ', leading to a total pulse train duration of T. Each pulse is typically at relatively high field ($B_1^{D\text{-}CEST}$, in Hz) and of duration τ_p

[a] Dr. T. Yuwen, Prof. L. E. Kay
Departments of Molecular Genetics, Biochemistry and Chemistry, University of Toronto, Toronto, Ontario M5S 1A8, Canada
[b] Prof. L. E. Kay
Hospital for Sick Children, Program in Molecular Medicine, 555 University Avenue, Toronto, Ontario M5G 1X8, Canada
[c] Dr. G. Bouvignies
Laboratoire des biomolécules, LBM, Département de chimie, École normale supérieure, PSL University, Sorbonne Université, CNRS, 75005 Paris, France
E-mail: guillaume.bouvignies@ens.fr

[**] CEST: Chemical Exchange Saturation Transfer

Supporting information for this article is available on the WWW under https://doi.org/10.1002/cphc.201800249

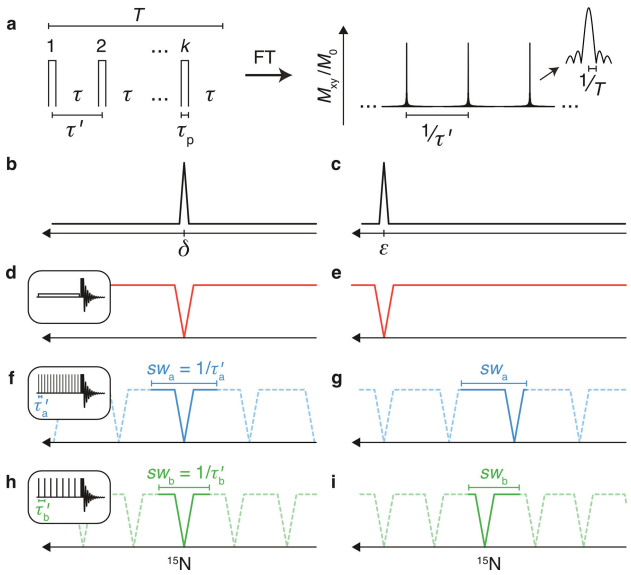

Figure 1. a) Schematic illustrating the DANTE pulse-train comprising k short pulses applied at intervals of τ' (left), along with the corresponding magnitude mode excitation profile in the frequency domain ($\sqrt{A(\omega)^2 + D(\omega)^2}$, where A and D are the absorptive and dispersive mode signals) generated by Fourier transform of the time domain scheme (right). More details are provided in SI. **b–i**) Comparison of regular and DANTE-based CEST profiles for a single non-exchanging spin resonating at positions δ (**b**, **d**, **f**, **h**) or ε (**c**, **e**, **g**, **i**). Note that in the D-CEST approach there is a potential ambiguity in the position of the dips due to the sw_{CEST}-periodicity of excitation with dips often aliased into the acquired $-sw_{CEST}/2$ to $+sw_{CEST}/2$ frequency range (for example, dip in **e**). By recording a pair of D-CEST experiments with different spectral widths it is possible to resolve ambiguities in the true resonance position resulting from aliasing (see text). Dashed lines denote regions of the conventional CEST profile outside of the sw_{CEST} interval in D-CEST, highlighting the ambiguity in peak position.

such that $\tau_p \ll \tau'$. As described by Morris and Freeman[10] and in SI the excitation profile can be most easily appreciated by considering the Fourier transform of the pulse train and the resulting frequency profile consists of regions of excitation that are spaced by $1/\tau' = sw_{CEST}$ and that have widths that depend on T, as indicated in Figure 1a (Figure S1). Alternatively, a more detailed treatment, albeit less intuitive, based on numerical integration of the Bloch equations can be evoked that highlights the experimental requirements for effective DANTE excitation (Figure S2). Both approaches establish that for excitation of the complete bandwidth it is necessary only to vary the carrier over a range of frequencies corresponding to sw_{CEST}, rather than the total range of possible frequencies for a given spin-type as is currently done in typical CEST applications.[3] A schematic illustrating the new CEST scheme, referred to as D-CEST (DANTE-CEST), is shown in Figure 1b–i, considering a single spin that does not undergo exchange for simplicity. Two examples, corresponding to the spin resonance position in the center of the spectral window (b, frequency δ) or to the side (c, frequency ε) have been selected. In the standard CEST experiment (referred to as CEST in what follows), illustrated in the inset to panel d, CEST dips are obtained (d, e) at the positions of peaks in the 1D spectra (b, c). Consider now excitation via the D-CEST scheme with pulses spaced τ'_a apart (inset to f) and where the carrier frequency is swept from $-sw_a/2$ to $+sw_a/2$ centered about δ. In this case an identical profile to that in d is observed, albeit with considerable savings in time since only a fraction of the number of spectra are required relative to the experiment in d. Note that, in principle, it is not possible to ascertain whether the dip of interest derives from a peak centered at δ or at $\delta \pm k \cdot sw_a$, where k is a whole number, (aliasing, illustrated schematically by the dashed dips) from the single D-CEST experiment because an 'excitation' spectral width of sw_a is chosen that does not cover the whole bandwidth of possible resonance positions. However, the true position of the dip can be resolved by recording an additional experiment with a spectral width $sw_b \neq sw_a$, (h), corresponding to a different spacing between DANTE pulses (τ'_b *vs* τ'_a). In the case where the 'true' dip position lies outside sw_a (e), the dip will appear aliased into the spectral region, sw_a, as shown in g (continuous lines). By recording a second profile with a different spectral width, aliasing occurs at a different position (i) and from the combination of the two profiles it is straightforward to reconstruct the resonance frequency. This can be obtained from the position where dips in the blue (g) and green (i) profiles superimpose (Figure S3, SI text). Although the above discussion has focused on the use of DANTE-based excitation schemes, other approaches such as those involving cosine-modulated waveforms are also possible and these would be expected to perform equally well. Further discussion is provided in a separate paper.[11]

Figure 2 shows selected profiles from both ^{15}N CEST (a, b) and D-CEST (c–f) experiments, recorded using a previously described pulse scheme[3] and the one illustrated in Figure S4, respectively, for a pair of residues in the G48A Fyn SH3 exchanging system that has been studied previously.[8,12] In the CEST experiment a total of 133 points have been recorded in the CEST dimension, separated by 25 Hz (…, −25, 0, +25, …). A pair of D-CEST experiments has also been measured using different sw_{CEST} values (700 and 800 Hz) so as to remove degeneracies in the extracted chemical shifts of excited state nuclei. These were obtained by sampling every 50 Hz ($\pm(25+50p$ Hz) and $\pm 50p$ Hz, $p = 0, 1, 2, \ldots$) using an average B_1 field ($B_1^{D\text{-}CEST}\frac{\tau_p}{\tau'} =$ 20 Hz, Figure 1a) that is equivalent to that measured in the regular CEST scheme (B_1^{CEST} in Figure 2a, b; see SI). In many applications it will be more advantageous to record the two datasets with different average B_1 fields such that one is on the order of or smaller than k_{ex} that, in general, increases the accuracy of the extracted exchange parameters.[5,13] Thus, a pair of D-CEST experiments is recorded covering in total the same number of sampled frequencies as for CEST and since both D-CEST datasets are fit together there is no loss in information by using a 50 Hz spacing. Although the D-CEST profiles can look quite distinct for different choices of sw_{CEST} due to different aliasing patterns (compare d, f), the frequencies of the excited state dips are easily determined, as shown by the perfect correlation between ^{15}N chemical shift values extracted from fits of the CEST and D-CEST profiles using a 2-state exchange model (Figure S5). Notably, excellent agreement between exchange parameters is also obtained, with (p_E, k_{ex}) = (6.39 ± 0.01 %, 135.6 ± 0.7 s^{-1}) and (6.31 ± 0.01 %, 138.9 ± 0.9 s^{-1}) from the two approaches. It is most likely that the uncertainties in the

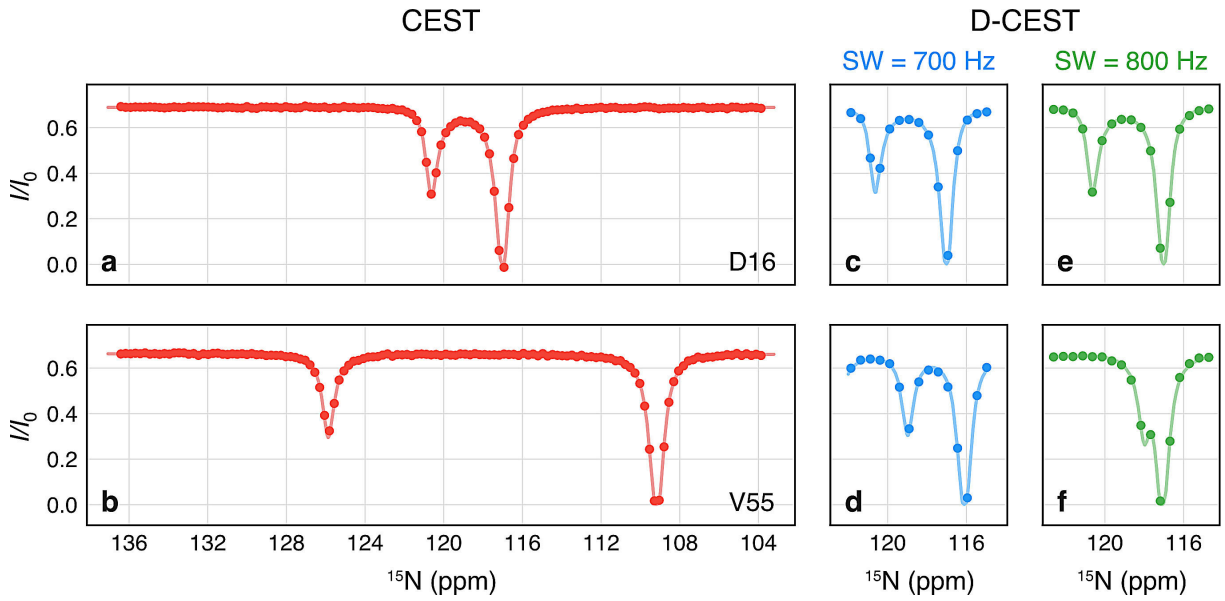

Figure 2. ^{15}N-CEST profiles of residues D16 (**a**, **c**, **e**) and V55 (**b**, **d**, **f**) of the G48A Fyn SH3 domain recorded at 25 °C, 23.5 T, using the standard ^{15}N-CEST pulse sequence (red) (**a**, **b**) and the ^{15}N D-CEST pulse sequence with sw_{CEST} set to 700 Hz (blue) (**c**, **d**) and 800 Hz (green) (**e**, **f**). All experiments were recorded with the same carrier position (~118.7 ppm) with B_1 offset ranges in the CEST (sw = 3300 Hz), D-CEST (sw = 700 Hz) and D-CEST (sw = 800 Hz) datasets of [−1500, 1800] Hz, [−375, 325] Hz and [−400, 400] Hz, respectively. Experimental data points are shown with circles along with best fits of data (solid lines). D-CEST datasets were jointly analyzed as described in SI. All experiments were recorded using an effective B_1 field of 20 Hz.

(p_E, k_{ex}) values reported here based on a covariance matrix approach,[14] and similar to values obtained from a Monte Carlo analysis,[14] underestimate the true errors that include systematic effects, such as a slight B_1 miscalibration, for example. Finally, the D-CEST method provides a greater than four fold acceleration in data collection in this particular case since a 3300 Hz spectral window is recorded in the CEST dimension in the regular CEST experiment (1 GHz static magnetic field) while an average window of 750 Hz is used for D-CEST. This acceleration was achieved without any compromise in sensitivity or information content.

Perhaps the greatest advantage of the D-CEST scheme is realized for applications involving exchanging systems with small chemical shift differences between states or in studies where there is a need to focus on residues with small shift differences. In these cases very weak CEST B_1 fields must be used as the widths of the resulting dips scale with B_1.[15] This is illustrated with an application to the A39G FF domain from human HYPA/FBP11, focusing on residues with small differences in chemical shifts between the exchanging states. Figure 3a–d illustrates select ^{15}N D-CEST profiles (blue) recorded using a 5 Hz B_1 field; the profiles have been circularly shifted so that the major dips appear at their true position. By means of comparison, the corresponding profiles from a standard CEST experiment recorded with $B_1 = 20$ Hz are shown (red). It is clear that the minor state dips are obscured from those of the major state. The complete CEST traces for the illustrated residues are shown in the bottom set of panels. Notably, a spectral width of 240 Hz was used for the ^{15}N D-CEST experiment in this case, in comparison to 2000 Hz for the regular CEST, corresponding to an approximate 8 fold savings in measurement time. In this case, however, a second CEST profile would be required with both a larger spectral width and a larger B_1 field to (i) minimize overlap between aliased minor and major dips and (ii) increase the intensity of the minor dips so as to obtain accurate estimates for (p_E, k_{ex}) values.

Although the experiments described above focus on ^{15}N D-CEST it is possible to exploit the DANTE approach in studies involving other probes of conformational exchange such as ^{13}C, for example, in cases where isolated ^{13}C spins can be incorporated into the molecule of interest. It is noteworthy, however, that in [U-^{13}C]-labeled molecules the presence of large one-bond ^{13}C–^{13}C scalar couplings can be detrimental, unlike the case for CEST applications involving continuous-wave excitation elements where the highly selective nature of the weak B_1 field ensures that only one spin is perturbed at a time.[12,16]

In summary, we have presented a simple frequency-selective based CEST scheme that builds on the DANTE sequence first proposed over 40 years ago.[9] The approach is easy to implement and the results can be analyzed in a straightforward manner using software that is available upon request (https://github.com/gbouvignies/chemex). The method can be combined with NUS approaches[17] resulting in further savings in measurement times, as has been recently described in the context of pseudo-4D CEST applications.[18] Even without NUS, the D-CEST experiment offers very significant decreases in measurement times, by as much as an order of magnitude in certain applications, and as such it will be a powerful addition to the repertoire of experiments that probe biomolecular dynamics.

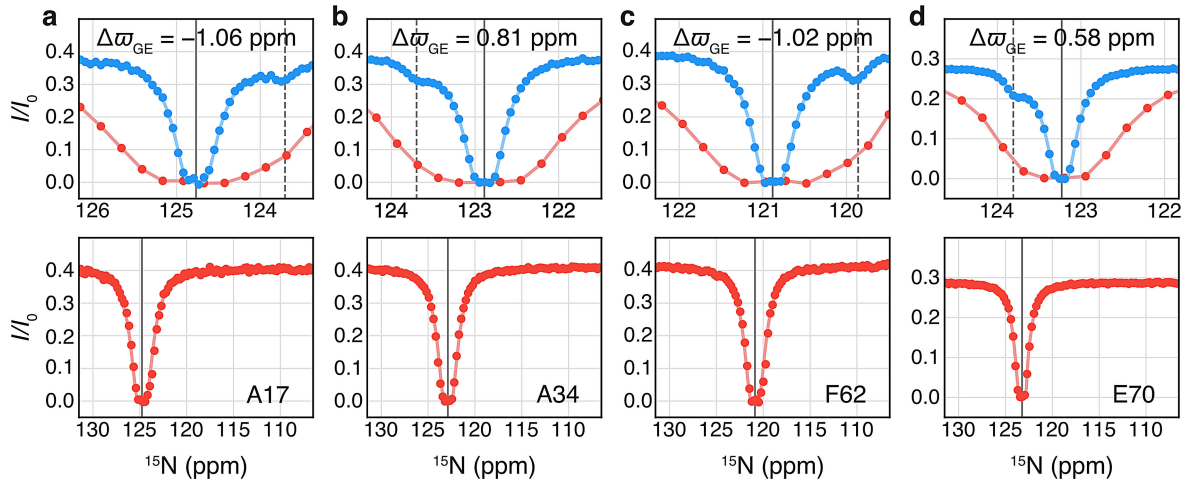

Figure 3. Selected CEST (red, 20 Hz B_1) and D-CEST profiles (blue, 5 Hz B_1) recorded on a sample of the A39G FF domain, 1 °C, 18.8 T with (p_E, k_{ex}) = (1.65 ± 0.02 %, 51.6 ± 1.0 s^{-1}).[3] Experimental data points are shown with circles along with best fits of data (solid lines), and the positions of the major and minor dips are highlighted with solid and dashed gray vertical lines, respectively. The chemical shift differences (ppm) between ground (*G*) and excited (*E*) states, $\Delta\varpi_{GE} = \varpi_E - \varpi_G$, are indicated. Profiles in the top panels have been circularly shifted so that the major dip lies in the center of the spectral window.

Acknowledgments

Financial support from the CNRS and TGIR-RMN-THC Fr3050 CNRS is gratefully acknowledged by G.B. and from the Canadian Institutes of Health Research (CIHR), grant number MFE-152561 and the Natural Sciences and Engineering Research Council of Canada (NSERC) by L.E.K. T.Y. acknowledges post-doctoral support from the CIHR. L.E.K. holds a Canada Research Chair in Biochemistry.

Conflict of Interest

The authors declare no conflict of interest.

Keywords: CEST · DANTE excitation · excited protein states · NMR spectroscopy · proteins

[1] S. Forsén, R. A. Hoffman, *J. Chem. Phys.* **1963**, *39*, 2892–2901.
[2] K. M. Ward, A. H. Aletras, R. S. Balaban, *J. Magn. Reson.* **2000**, *143*, 79–87.
[3] P. Vallurupalli, G. Bouvignies, L. E. Kay, *J. Am. Chem. Soc.* **2012**, *134*, 8148–8161.
[4] B. Zhao, Q. Zhang, *J. Am. Chem. Soc.* **2015**, *137*, 13480–13483.
[5] P. Vallurupalli, A. Sekhar, T. Yuwen, L. E. Kay, *J. Biomol. NMR* **2017**, *67*, 243–271.
[6] H. M. McConnell, *J. Chem. Phys.* **1958**, *28*, 430–431.
[7] P. Jemth, R. Day, S. Gianni, F. Khan, M. Allen, V. Daggett, A. R. Fersht, *J. Mol. Biol.* **2005**, *350*, 363–378.
[8] A. A. Di Nardo, D. M. Korzhnev, P. J. Stogios, A. Zarrine-Afsar, L. E. Kay, A. R. Davidson, *Proc. Natl. Acad. Sci. USA* **2004**, *101*, 7954–7959.
[9] G. Bodenhausen, R. Freeman, G. A. Morris, *J. Magn. Reson.* **1976**, *23*, 171–175.
[10] G. A. Morris, R. Freeman, *J. Magn. Reson.* **1978**, *213*, 214–243.
[11] T. Yuwen, G. Bouvignies, L. E. Kay, *J. Magn. Reson.* **2018**, *292*, 1–7.
[12] G. Bouvignies, P. Vallurupalli, L. E. Kay, *J. Mol. Biol.* **2014**, *426*, 763–774.
[13] M. G. Carneiro, J. G. Reddy, C. Griesinger, D. Lee, *J. Biomol. NMR* **2015**, *63*, 237–244.
[14] W. Press, B. Flannery, S. Teukolsky, W. Vetterling, *Numerical Recipes: The Art of Scientific Computing*, **1986**.
[15] M. Zaiss, P. Bachert, *Phys. Med. Biol.* **2013**, *58*, R221–R269.
[16] P. Vallurupalli, G. Bouvignies, L. E. Kay, *ChemBioChem* **2013**, *14*, 1709–1713.
[17] M. Mobli, J. C. Hoch, *Prog. Nucl. Magn. Reson. Spectrosc.* **2014**, *83*, 21–41.
[18] D. Long, F. Delaglio, A. Sekhar, L. E. Kay, *Angew. Chem. Int. Ed. Engl.* **2015**, *54*, 10507–10511.

Manuscript received: March 20, 2018
Accepted Article published: April 17, 2018
Version of record online: May 24, 2018